Environmental Science & Technology

pubs.acs.org/est

Article

Antimony Isotope Fractionation Revealed from EXAFS during Adsorption on Fe (Oxyhydr)oxides

Weiqing Zhou, Jianwei Zhou, Xinbin Feng, Bing Wen, Aiguo Zhou, Peng Liu,* Guangyi Sun,* Ziyi Zhou, and Xin Liu

Cite This: *Environ. Sci. Technol.* 2023, 57, 9353−9361

Read Online

ACCESS | Metrics & More | Article Recommendations | Supporting Information

ABSTRACT: A lack of knowledge about antimony (Sb) isotope fractionation mechanisms in key geochemical processes has limited its environmental applications as a tracer. Naturally widespread iron (Fe) (oxyhydr)oxides play a key role in Sb migration due to strong adsorption, but the behavior and mechanisms of Sb isotopic fractionation on Fe (oxyhydr)oxides are still unclear. Here, we investigate the adsorption mechanisms of Sb on ferrihydrite (Fh), goethite (Goe), and hematite (Hem) using extended X-ray absorption fine structure (EXAFS) and show that inner-sphere complexation of Sb species with Fe (oxyhydr)oxides occurs independent of pH and surface coverage. Lighter Sb isotopes are preferentially enriched on Fe (oxyhydr)oxides due to isotopic equilibrium fractionation, with neither surface coverage nor pH influencing the degree of fractionation ($\Delta^{123}Sb_{aqueous\text{-}adsorbed}$). Limited Fe atoms are present in the second shell of Hem and Goe, resulting in weaker surface complexes and leading to greater Sb isotopic fractionation than with Fh ($\Delta^{123}Sb_{aqueous\text{-}adsorbed}$ of 0.49 ± 0.004, 1.12 ± 0.006, and 1.14 ± 0.05‰ for Fh, Hem, and Goe, respectively). These results improve the understanding of the mechanism of Sb adsorption by Fe (oxyhydr)oxides and further clarify the Sb isotope fractionation mechanism, providing an essential basis for future application of Sb isotopes in source and process tracing.

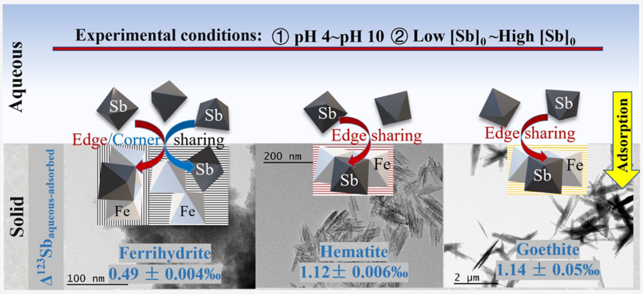

KEYWORDS: *antimony, adsorption, Fe (oxyhydr)oxides, isotope fractionation, EXAFS*

■ INTRODUCTION

Antimony (Sb) is a potentially toxic and carcinogenic metalloid, and Sb pollution caused by natural processes and human activities is widely present in soil and water environments.[1,2] Understanding the geochemical characteristics of Sb is a prerequisite for the prediction and remediation of Sb pollution. Sb isotopes have potential applications as a new and powerful tool to reveal information about the sources, transformation mechanisms, and transport of Sb, such as precipitation and dissolution, evaporation and condensation, oxidation and reduction, adsorption and desorption, mixing, and microbial processes.[3] The transport of Sb in geochemical processes is often strongly controlled by mineral adsorption,[4] and the identification of the corresponding fractionation factors is key to interpreting the natural Sb isotopic signature.

Iron (Fe) (oxyhydr)oxides are commonly associated with a variety of aquatic systems, soils, and sediments and include highly reactive natural minerals such as ferrihydrite (Fh), goethite (Goe), and hematite (Hem) that play important roles in the immobilization of Sb.[5] Mitsunobu et al.[6] report edge and corner-sharing complexes when Sb adsorbs on Fh, while Guo et al.[7] only report edge-sharing complexes. X-ray absorption fine structure (EXAFS) results show the $Sb(OH)_6^-$ octahedron shares an edge with Goe at pH 7.5 and 3.2.[6,8] The envelope of Sb(V) adsorbed on Goe has been simulated using the triple layer model (TLM), based on monodentate and bidentate complexes at pH < 7 and pH > 7, respectively.[9] Crystal truncation rod X-ray diffraction showed Sb is bound by edge and corner-sharing on Hem at pH 5.5.[10] Recently, Mierzwa et al.[11] concluded that Sb adsorbs on Hem as inner and outer-sphere surface complexes at pH 5−7 but only as an outer-sphere complex at pH 8. These studies reveal Sb(V) complexes with Fh as a strong inner-sphere complex, whereas the inner- and outer-sphere complexes formed with Hem and Goe are pH-dependent. The inconsistent conclusions reached in these studies are due to the different Sb/Fe molar ratios, mineral types, and analysis methods (Table S1). More recently, studies have also focused on the interaction mechanism between Sb(V) and Fe(III) minerals such as jarosite and schwertmannite using EXAFS.[12,13] However, direct evidence of the complexation mechanism with varying

Received: March 11, 2023
Revised: May 25, 2023
Accepted: May 26, 2023
Published: June 9, 2023

https://doi.org/10.1021/acs.est.3c01906
Environ. Sci. Technol. 2023, 57, 9353−9361

pH or surface coverage conditions is lacking. Therefore, the mechanism of Sb adsorption on Fe (oxyhydr)oxides needs further clarification.

The stable isotopes of Sb, ^{121}Sb, and ^{123}Sb have natural abundances of 57.213 and 42.787%, respectively.[14] Rouxel et al.[15] report large isotopic fractionation (0.9‰) when pentavalent Sb is reduced to trivalent Sb. Subsequent related studies on Sb isotopes focus on analysis methods,[16−21] tracing of ancient glass,[22−25] mining environments,[26−29] and hydrothermal systems.[30] These studies indicate Sb isotope is an effective tracer of contamination sources and geochemical processes, but the mechanisms and factors controlling isotope fractionation during the migration and transformation of Sb are still unclear. We recently reported that no significant isotopic fractionation occurs during Sb(V) adsorption by γ-alumina.[31] However, Sb isotope fractionation is important during adsorption on Fe (oxyhydr)oxides. For example, Tanimizu et al.[27] attribute heavy Sb isotope enrichment from mine drainage to the adsorption of Sb on Fe (oxyhydr)oxides, but the isotope fractionation mechanisms in the corresponding process need to be verified with experimental studies.

The mechanism of Sb adsorption by different Fe (oxyhydr)oxides under various experimental conditions may be different, which is likely to result in distinct degrees of Sb isotope fractionation. However, these processes have not been thoroughly investigated. This study reveals the adsorption mechanisms and isotopic fractionation behaviors of Sb(V) adsorbed on Fe (oxyhydr)oxides (Fh, Goe, and Hem) under various pH conditions and initial Sb concentrations. The study aimed to determine the (1) adsorption mechanisms of Sb(V) by different Fe (oxyhydr)oxides, (2) isotope fractionation mechanism of Sb(V) by different Fe (oxyhydr)oxides, and (3) effect of pH and initial Sb concentration on Sb isotope fractionation. The results will contribute to understand the environmental fate of Sb and facilitate applications of Sb isotopes as tracers of geochemical processes.

■ MATERIALS AND METHODS

Materials. Sb(V) stock solution (200 mg L^{-1}) was created from $KSbH_6O_6$ (Wako Pure Chemical Industries, Ltd.) and ultrapure water (MQ, 18.2 MΩ). $Fe(NO_3)_3\cdot 9H_2O$ (98.5−100%), KOH (≥99.9%), and HNO_3 (65−68%) were purchased from Sinopharm Chemical Reagent Co., Ltd., China. An Sb standard solution (NIST SRM 3102a) was used as a quality control standard for isotope analysis. High-purity Sb solution from Alfa Aesar (USA; lot: 1227270B) was used as the secondary standard solution. The cation exchange resin AG50W-X8 (200−400 mesh) and 10 mL polypropylene columns were from Bio-Rad. Silica-based thiol resin (Cleanert SH, pore size: 60 Å, grain size: 40 μm) was from Tianjin Bonna-Agela Technologies (China). All acids used during Sb isotope purification were purified twice. Fh, Hem, and Goe were synthesized according to a previously published method,[32] with detailed preparation information provided in the Supporting Information (SI).

Adsorption Experiments. The working solutions for the three batch experiments (kinetic, isothermal, adsorption edge) as well as the suspensions of Fe (oxyhydr)oxides hydrated for 24 h were adjusted with 1 M HNO_3/KOH until a set pH was maintained. The experiment began by mixing the working solution and suspension. During the subsequent adsorption process, the pH of the system was slightly adjusted to the desired value several times. The volume of HNO_3/KOH used for pH adjustment was negligible in these experiments. The ionic background for all batch experiments was 0.01 M KNO_3. All experiments were carried out in high-density polyethylene bottles with shaking at 120 rpm at a constant temperature (25 °C). The suspensions were subjected to centrifugation at 3000 rpm for 1 min. The resulting supernatants were filtered using polyether sulfone filters with a pore size of 0.22 μm (Merck Millipore, Germany) and acidified using HNO_3 (pH < 2). The centrifuged solid samples were freeze-dried before EXAFS measurements. Unfiltered aqueous sample was measured for pH (Orion 9678BNWP).

For the kinetic experiments (5 min to 48 h in duration), 5.83, 11.37, and 20.31 mg L^{-1} Sb working solutions were reacted at pH 6.5 with 1 g L^{-1} Goe, 1 g L^{-1} Hem, or 0.6 g L^{-1} Fh, respectively. The suspensions were collected at set time intervals (Table S2). The isothermal experiments were conducted at pH 6.5 for 48 h using different initial Sb concentrations (1.17 to 35.06 mg L^{-1} for 1 g L^{-1} Goe, 6.59 to 59.09 mg L^{-1} for 1 g L^{-1} Hem, and 4.90 to 56.23 mg L^{-1} for 0.6 g L^{-1} Fh). For the adsorption edge experiments (pH 4−10), 5.71, 12.06, and 22.56 mg L^{-1} Sb working solutions were reacted with 1 g L^{-1} Goe, 1 g L^{-1} Hem, or 0.6 g L^{-1} Fh, respectively. Replicate experiments (2 or 3) were carried out to ensure reproducibility (Tables S2 and S3). Pseudo-first-order (PFO) and pseudo-second-order (PSO) models were used to fit the kinetic data, while Langmuir and Freundlich models were used to fit the isothermal data. Detailed fitting and calculation methods are provided in the SI.

Analysis Methods. The Sb concentration was analyzed by hydride generator-atomic fluorescence spectroscopy (HG-AFS; Haiguang, China). The method of Sb speciation using Visual MINTEQ 3.1[33] as a function of pH is provided in the SI. Brunauer−Emmett−Teller (BET), X-ray diffraction (XRD), and transmission electron microscopy (TEM) methods and results from the analysis of the synthetic Fe (oxyhydr)oxides are also provided in the SI (see text and Figures S1−S3). Solid samples from the kinetic, isothermal, and adsorption edge experiments were packed in 2 mm thick polytetrafluoroethylene (PTFE) holders sealed by Kapton tape in preparation for EXAFS analysis. The EXAFS experiments were conducted at the Advanced Photon Source (APS) Beamline 20-BM. The EXAFS spectra were processed and analyzed using the Demeter software package.[34] A linear function was subtracted from the pre-edge region, and then the edge jump was normalized using ATHENA software.[34] The $\chi(k)$ data were isolated by subtracting a smooth, three-term polynomial approximating the absorption background. All spectra were aligned with the simultaneous measurement of a reference material with known E_0. EXAFS modeling was conducted by nonlinear fitting, with least-squares refinement, of the EXAFS equation to the Fourier-transformed (FT) data in R-space with ranges of 2.5−10.5 Å, using ARTEMIS software.[34] The k^3-weighted $\chi(k)$ data were Fourier-transformed after applying a Hanning window function in a k range of 2.5−10.5 $Å^{-1}$. The tripuhyite ($FeSbO_4$) structure file for EXAFS modeling was obtained from the American Mineralogist Crystal Structure Database.[35] The amplitude reduction factor (S_0^2, 0.85) was fixed according to the fits to reference spectra ($K_2H_2Sb_2O_7\cdot 4H_2O$) that was measured at the same run of the sample measurement. The coordination numbers (CNs) for each shell, Debye−Waller factor (σ^2), and interatomic distance (ΔR) for each path were variables. The value of the threshold energy difference (ΔE_0) was considered identically

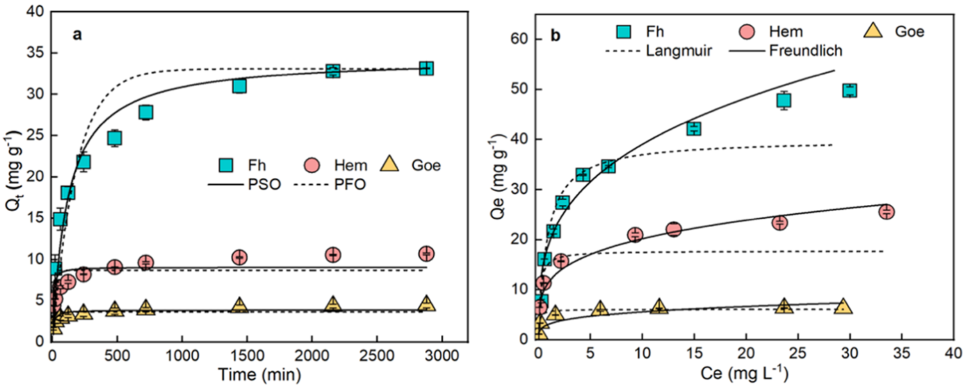

Figure 1. Behavior of Sb adsorbed by Fe (oxyhydr)oxides based on kinetic experiments (a) and isothermal experiments (b). Q_t represents Sb adsorbed on Fe (oxyhydr)oxides at time t; Q_e represents the amount of Sb adsorbed on Fe (oxyhydr)oxides at adsorption equilibrium; and C_e is the Sb concentration in the aqueous phase after adsorption equilibrium.

for each path. The fitting was employed to obtain the CNs, ΔE_0, f, σ^2, ΔR, and goodness of fit (R-factor). Detailed methods with respect to sample preparation, beamline instrumentation and setup, and methods of data collection and fitting results evaluation are provided in the SI and previous studies.[36,37]

Sb Isotope Analysis by MC-ICP-MS. Sb isotope samples were collected during the kinetic, isothermal, and adsorption edge experiments and subjected to isotope separation and purification methods mainly based on previous reports.[20] Ion exchange chromatography combined with a thiol resin column was used for the separation and purification of Sb isotopes. Before loading the column, approximately 30−100 ng of Sb from the sample solution was placed in a polyfluoroalkoxy (PFA) cup and evaporated on a hotplate at 90 °C until almost dryness. After adding 0.4 mL of H_2O_2 and 0.6 mL of HNO_3 to the PFA cup, the samples were digested at 100 °C for 0.5 h and evaporated at 90 °C until almost dryness. Each sample was dissolved with 1 mL of 0.15 M HF for 15 min at 90 °C until no residue was left in the solution. The digested samples were processed through AG50W-X8 cation resin and then through thiol resin to remove matrix (K and Fe) and interfering elements. Detailed methods with the steps for column chemistry are provided in the SI. Quality control for each experiment was performed using standard and blank solutions.[20]

Purified samples were imported into a multi-collector inductively coupled plasma mass spectrometer (MC-ICP-MS) using a hydride generation priming system with a PFA nebulizer (aspiration rate: 50 μL min^{-1}). The volume of the solution and the Sb concentration were 6 mL and 3 ng mL^{-1}, respectively, for the isotopic analysis. Sb isotopes were analyzed with a Nu Plasma II MC-ICP-MS (Nu Instruments Ltd., UK). Instrument background and acid matrix blanks were corrected by performing on-peak acid blank measurements for precise Sb isotope analysis. The instrument parameters used for Sb isotope ratio measurements are shown in Table S4. The Sb isotopic composition (δ^{123}Sb) was calculated relative to the Sb standard solution (NIST SRM 3102a) using the following equation

$$\delta^{123}\mathrm{Sb} = \left\{ \frac{(^{123}\mathrm{Sb}/^{121}\mathrm{Sb})_{\mathrm{sample}}}{(^{123}\mathrm{Sb}/^{121}\mathrm{Sb})_{\mathrm{standard}}} - 1 \right\} \times 1000 \tag{1}$$

The NIST 3102a standard reference material was measured every three samples to check the stability of the instrument. ^{111}Cd and ^{113}Cd isotopes were used to correct the instrumental mass bias.[20] The Long-term analytical precision was 2sd < 0.04‰. The in-session analytical precision, based on the δ^{123}Sb content of the secondary Sb standard solution (Alfa Aesar; lot: 1227270B), was 0.282 ± 0.039‰. The same samples were measured twice, and then the 2sd values were calculated. The δ^{123}Sb on the adsorbed phase was obtained according to the mass balance equation

$$\delta^{123}\mathrm{Sb}_{\mathrm{adsorbed}} = (\delta^{123}\mathrm{Sb}_{\mathrm{stock}} - \delta^{123}\mathrm{Sb}_{\mathrm{aqueous}} \times (1 - f))/f \tag{2}$$

The Sb isotopic fractionation (Δ^{123}Sb aqueous-adsorbed) between the adsorbed phase and aqueous phase is denoted as

$$\Delta^{123}\mathrm{Sb}_{\mathrm{aqueous-adsorbed}} = \delta^{123}\mathrm{Sb}_{\mathrm{aqueous}} - \delta^{123}\mathrm{Sb}_{\mathrm{adsorbed}} \tag{3}$$

where "f" represents the fraction of Sb adsorbed. $\delta^{123}\mathrm{Sb}_{\mathrm{stock}}$, $\delta^{123}\mathrm{Sb}_{\mathrm{adsorbed}}$, and $\delta^{123}\mathrm{Sb}_{\mathrm{aqueous}}$ represent the δ^{123}Sb value of the stock solution, adsorbed phase samples, and aqueous phase samples, respectively.

■ RESULTS AND DISCUSSION

Adsorption Behavior of Sb on Fe (Oxyhydr)oxides. *Kinetic and Isothermal Adsorption.* The amount of Sb in the adsorbed phase increased with time and reached adsorption equilibrium at 24 h (Figure 1a). The PSO model is more suitable for representing the adsorption characteristics of Sb with Fh, Hem, and Goe (R^2 = 0.973, 0.922, and 0.911, respectively) than the PFO model (R^2 = 0.897, 0.861, and 0.714, respectively) (Table S5). The equilibrium amount of Sb adsorbed on Fh, Hem, and Goe after 48 h (33.16, 10.6, and 3.94 mg g^{-1}, respectively) is close to that predicted by the PSO model (34.4, 9.05, and 3.89 mg g^{-1}, respectively). Chemisorption is the main mechanism according to the fitting results of the PSO model. Previous research shows the PSO model is more suitable for the kinetic adsorption of Sb(V) by freshly prepared Fh,[38] which is consistent with our results.

The amount of Sb adsorbed by the Fe (oxyhydr)oxides in the isothermal experiments gradually increased with increasing initial Sb concentration (Figure 1b). The adsorption behavior of Sb on Fh, Hem, and Goe is better fitted by the Freundlich model (Table S6; R^2 = 0.999, 0.946, and 0.981, respectively) than the Langmuir model, indicating the occurrence of a multilayer process. Previous research concludes the parameter *n* (1−10) in the Freundlich model suggests a favorable adsorption process, with an *n* value greater than 1 implying a heterogeneous adsorbent surface.[39] Therefore, the three Fe (oxyhydr)oxides exhibit heterogeneous surfaces and adsorption sites with different adsorption capacities, resulting in Freundlich model fitting *n* values of 3.26 for Fh, 4.14 for Hem, and 3.95 for Goe.

Effect of pH. The amount of Sb adsorbed on the three Fe (oxyhydr)oxides decreased as the pH increased from 3 to 10 (Figure 2). The amount of Sb adsorbed on Fh was ∼39.2 mg g^{-1} at pH < 7 and then decreased from 32.2 to 9.33 mg g^{-1} as the pH increased from 7 to 10. The amount of Sb adsorbed on Hem showed a similar trend, with > 11.9 mg g^{-1} under acidic conditions but 4.87 mg g^{-1} at pH = 10. The amount of Sb adsorbed on Goe decreased from 5.41 to 0.863 mg g^{-1} as the pH shifted from an acidic to a basic environment.

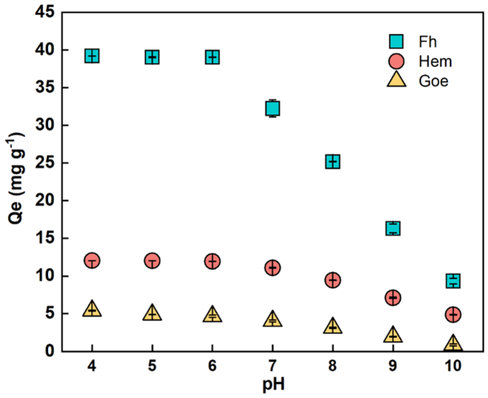

Figure 2. Behavior of Sb adsorbed on Fe (oxyhydr)oxides from adsorption edge experiments under different pH conditions. Q_e represents the amount of Sb adsorbed on Fe (oxyhydr)oxides at equilibrium.

pH is an important parameter controlling the metal adsorption process due to its impact on metal species in solution and the surface properties of the adsorbent.[40] The adsorbent surface is usually negatively charged when the pH is higher than the point of zero charge (PZC) and positively charged when the pH is lower than the PZC.[4] The repulsive interaction between Sb(OH)$_6^-$ and the adsorbent surface gradually increases when the pH rises above the PZC, which in turn weakens the adsorption of Sb(V), and *vice versa*. Previous studies show ζ potential values decrease in the order Goe > Hem > Fh at any pH value, with PZC values of 9.7, 9.8, and 8.5, respectively.[41] Sb(OH)$_6^-$ is the predominant antimonate species in the experimental pH range (4−10) based on the pC-pH diagram of Sb (Figure S4). In this study, the curve of the Sb adsorption content for the three minerals shows the same trend as the ζ potential, indicating pH affects the surface potential of the three minerals and indirectly controls Sb adsorption. In acidic environments, a positive ζ potential exists on the surface of the Fe (hydroxy)oxide due to the protonation process, and the negatively charged Sb(OH)$_6^-$ ions are promoted for adsorption by electrostatic forces. With increasing pH, the mineral surface deprotonation becomes more predominant, especially when the pH > pH$_{zpc}$ and the Fe (oxyhydr)oxide surface has a negative zeta potential, which increases the electrostatic repulsion with Sb and suppresses Sb adsorption. Therefore, the amount of Sb adsorbed on each oxide under acidic conditions is greater than under basic conditions. A similar observation was made for Sb on Fh, Goe, and Hem in previous adsorption edge studies.[7,11]

Bonding Structures of Sb Adsorbed on Fe (Oxyhydr)-oxides. The Fourier-transformed (FT) EXAFS spectra of the Fe (oxyhydr)oxides all show a first high-intensity peak at ∼1.98 Å, with the intensity and position of this peak not varying with adsorption conditions (Figures 3, S5, and S6). The spectral modeling results show this first peak represents about six O atoms with an average distance from the central Sb atom of 1.97−1.98 Å (Tables S7−S9). The Sb−O bond length aligns with the distance published in a previous study,[42] but some *CN* values are higher than theoretical values. This is due to the correlation of the *CN* with the S_0^2 and σ^2, which results in an uncertainty of the fitting method itself and does not affect the analysis of EXAFS data.[43]

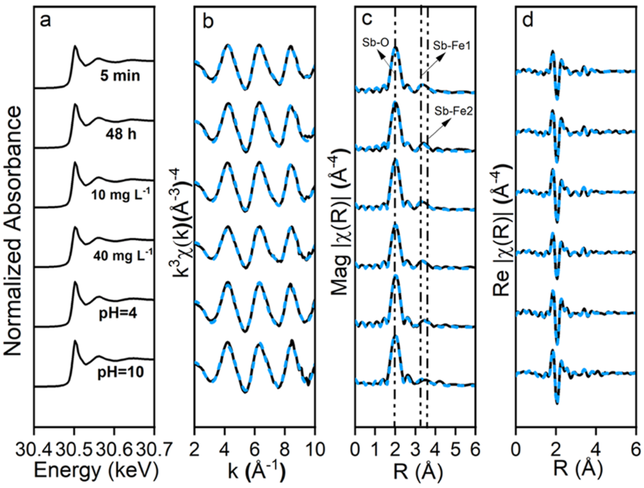

Figure 3. Sb K-edge EXAFS spectra and fitting results for kinetics, isothermal, and adsorption edge experiments related to Sb adsorption on Fh. Normalized XANES spectra (a), K^3 weighted EXAFS spectra (black solid) and fitting curve (blue dotted lines) (b), FT spectra and fitting curve (c), and FT spectra and fitting curve (d).

The intensity and position of two peaks located at ∼3.1 and ∼3.5 Å in the FT EXAFS spectra of Fh do not vary with adsorption conditions (Figure 3) and are consistent with the scattering signal associated with iron atoms.[6] The spectral modeling results indicate the CNs of Sb−Fe1 and Sb−Fe2 with atomic distances of 3.10−3.12 Å and 3.56−3.58 Å are 0.9−1.2 and 1.1−1.4, respectively (Table S7). The Sb−Fe bond distance is consistent with previous studies,[6,42] which indicates Sb adsorbs on Fh and forms edge and corner-sharing complexes. The modeling results from the isothermal experiment suggest the form of surface complexation is independent of the surface coverage, which is consistent with the findings of a previous study.[6] In addition, the spectral modeling results further confirm the form of the Sb complex on Fh is unaffected by adsorption time and pH, in agreement with the results of a previous study.[6]

The peak located at ∼3.1 Å in the FT spectra of Hem is consistent with the scattering signal of Fe atoms from the Sb−Fe$_1$ shell of Fh, and the intensity and position of the peaks are independent of loading levels and pH (Figure S5). The spectral modeling results show an atomic distance of 3.08 Å for Sb−Fe with CNs of 1.15−1.52 (Table S8). This distance is consistent with the Sb−Fe distance when the Sb(OH)$_6$

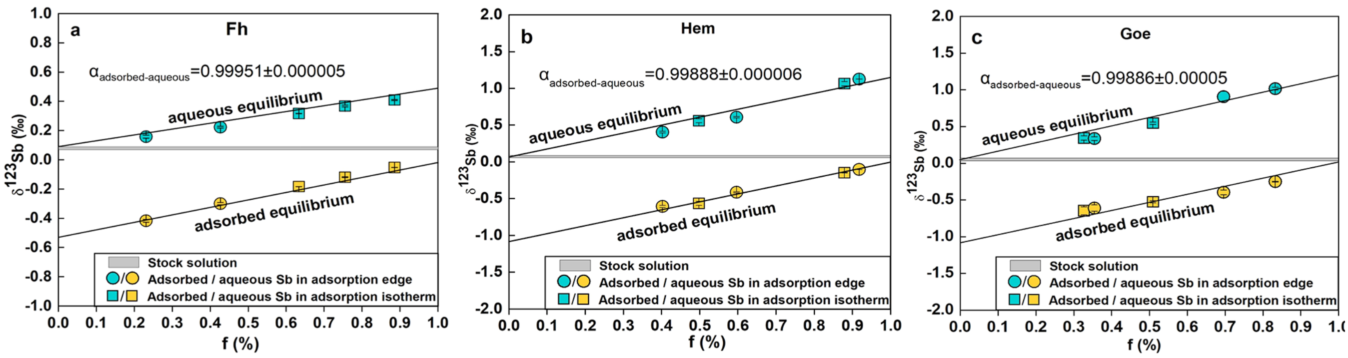

Figure 4. Isotopic fractionation behavior of Sb during adsorption on Fh (a), Hem (b), and Goe (c). The gray-shaded and black lines represent the δ^{123}Sb of the stock solution and the equilibrium fractionation model, respectively.

octahedra and $Fe(OH)_6$ octahedra share an edge, indicating Sb forms an inner-sphere complex with a shared edge on Hem. Previous studies using crystal truncation rod X-ray diffraction report similar results for Sb and Hem at pH 5.5.[10] However, Mierzwa et al.[11] demonstrate inner- and outer-sphere complexation at pH 5−7 yet only outer-sphere complexation at pH 8 using attenuated total reflectance Fourier transform infrared (ATR-FTIR) spectroscopy and surface complexation modeling. This differs from our results under alkaline conditions, likely due to the different Sb/Fe molar ratios and characterization methods. The previous study used a lower initial Sb concentration (1 mg L^{-1}) compared to the present study (10 mg L^{-1}), resulting in a smaller amount of Sb adsorbed onto the Hem under alkaline conditions. Therefore, the inconsistency with respect to the complexation form of Sb adsorption by Hem based on macroscopic and *in situ* ATR-FTIR results suggests the need for further investigation.

The FT EXAFS spectra of Sb(V) adsorbed by Goe show a peak at ∼3.1 Å that is due to the scattering of Fe atoms, similar to observations noted above for Hem (Figure S6). The intensity and position of the peaks do not vary with adsorption conditions, implying the Sb complexed on Goe is unaffected by adsorption time, pH, or surface coverage. The fitted Sb−Fe bond distances and CNs are 3.03−3.06 Å and 0.46−0.62, respectively (Table S9), indicating Sb forms edge-sharing complexes on Goe. Likewise, Scheinost et al.[8] and Mitsunobu et al.[6] used EXAFS to confirm the existence of an edge-sharing complex of Sb on Goe at pH 3.2 and 7.5, respectively, and Mitsunobu et al.[6] report the complex Sb forms with Goe is independent of surface coverage. In addition, our spectral modeling results do not vary with pH, which indicates stable inner-sphere complexation. These results concur with previous conclusions based on a triple layer model that indicates inner-sphere complexation of Sb(V) on Goe dominates at pH < 6, while outer-sphere complexation obviously increases at pH > 6.[44]

Sb Isotope Fractionation Behavior. Sb isotopes in the adsorbed and aqueous phases increase with increasing Sb adsorption ratios on the three Fe oxides (Figure 4). This observation shows lighter Sb isotopes are preferentially adsorbed onto the solid phase, causing the heavier isotope to remain in the aqueous phase. The fitting results of the equilibrium and Rayleigh models show the Sb isotopes in Fh, Hem, and Goe adsorption processes are all better described by equilibrium fractionation, with fractionation factors ($\alpha_{\text{adsorbed-aqueous}}$) of 0.99951 ± 0.000005, 0.99888 ± 0.000006, and 0.99886 ± 0.00005, respectively. The equilibrium fractionation model represents isotope exchange in a ″closed″ system, which implies adequate isotope exchange between the aqueous solution and oxide surface throughout the sorption experiments.[45] Therefore, the fitting results illustrate that the light and heavy Sb isotopes in the two phases react at the same forward and backward reaction rates and that the final isotopic fractionation is controlled by the energy difference in the bonding environments of the reactants that have reached isotopic equilibrium.[46]

Sb isotopic fractionation studies of adsorption processes generally require clarification of the Sb speciation in the aqueous phase and whether any phase shift occurs in the solid phase, as these changes are likely to result in isotope fractionation.[31] The structure of Fh as a precursor of Goe may change during the adsorption process due to the presence of labile Fe(III).[47] However, no significant phase transformation of Fh was noted based on XRD analysis after 48 h (Figure S1), which is consistent with the TEM analysis (Figure S2). Overall, the results show no independent (Sb-containing) minerals formed under the batch experimental conditions. In addition, $Sb(OH)_6^-$ is the dominant Sb species as a function of pH based on the Visual MINTEQ simulation (Figure S4), and the Sb species in solution does not vary due to the maintenance of a stable pH. Therefore, the Sb isotope fractionation behavior in this study is only related to the complex forms of Sb and the different Fe oxides.

Sb Isotope Fractionation Mechanism. The Sb isotopic fractionation for each oxide is not significantly different in the adsorption edge and isothermal adsorption experiments, but the fractionation values ($\Delta^{123}\text{Sb}_{\text{aqueous-adsorbed}}$) on Hem and Goe are similar and double that of Fh (Figure 5). Specifically, the $\Delta^{123}\text{Sb}_{\text{aqueous-adsorbed}}$ adsorbed on Fe (oxyhydr)oxides is 0.46 ± 0.004‰−0.54 ± 0.04‰ for Fh, 1.01 ± 0.03‰−1.23 ± 0.001‰ for Hem, and 1.05 ± 0.07‰−1.22 ± 0.1‰ for Goe. The theoretical $\Delta^{123}\text{Sb}_{\text{aqueous-adsorbed}}$ between aqueous Sb and adsorbed Sb can be calculated from $\alpha_{\text{adsorbed-aqueous}}$ for later comparative discussion and reference, yielding $\Delta^{123}\text{Sb}_{\text{aqueous-adsorbed}}$ values of 0.49 ± 0.004, 1.12 ± 0.006, and 1.14 ± 0.05‰ for Fh, Hem, and Goe, respectively. Changes in the bonding environment are the key reason for equilibrium isotope fractionation, with heavy isotopes tending to be enriched with "stiffer bonds," i.e., lower coordination numbers, shorter bonds, higher oxidation states, etc.[48,49] In our experiments, Sb was adsorbed on Fe (oxyhydr)oxides as an inner-sphere complex with a longer Sb−Fe bond than the Sb−O bond. Therefore, the lighter Sb isotope is preferentially adsorbed on Fe(oxyhydr)oxides. The same principle of

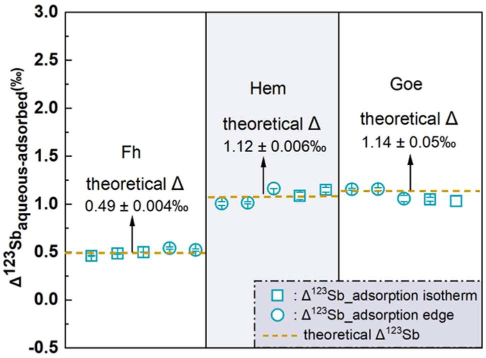

Figure 5. Isotopic fractionation value (Δ) of Sb during adsorption on Fh, Hem, and Goe. The yellow dashed line represents the theoretical fractionation value.

preferential adsorption for light isotopes is observed for the three Fe oxides, and similarly, adsorption of Ge,[50] Se,[51] Mo,[52,53] and U[54] has been found to lead to enrichment of light isotopes in the adsorbed phase.

The kinetic experiment for Sb adsorption by Fh showed no significant difference in Sb isotopes after 36 and 48 h (Table S10), which indicates the isotopic equilibrium time for Fh is less than 36 h. The equilibrium isotope exchange after the initial kinetic process normally occurs during the adsorption of metals on solids, and the time required for isotopic equilibrium is different than the time required for concentration equilibrium[46] and needs to be obtained based on kinetic adsorption experiments. Likewise, previous studies report that aqueous and adsorbed ions in Sb and Se kinetic adsorption experiments reach isotopic equilibrium relatively quickly (<30 h) and that kinetic and equilibrium fractionation occurs in these kinetic experiments.[31,51] In addition, Ge, W, and Mo adsorption on Fe and Mn oxides follows an equilibrium fractionation model that reaches isotopic equilibrium relatively quickly (<48 h).[55−58] Wasylenki et al.[59] reported that the amount of W adsorbed on birnessite and W isotope fractionation did not reach a steady state after ∼500 h in low ionic strength and low pH solutions. They infer that continuous growth of W−O surface precipitates occurs, and the nonequilibrium W isotopic fractionation is associated with the continued W uptake. However, the experiments in this study all reached Sb adsorption equilibrium within 48 h, and the EXAFS results show no anomalous spectra, so no kinetic isotope effects are superimposed on the equilibrium fractionation results for nonequilibrium isotopes. Therefore, the results herein indicate the Sb isotopic equilibrium time on Hem and Goe is less than 48 h due to their adsorption equilibrium time being much less than that for Fh.

The results of the isothermal experiment indicate no significant differences in Sb isotope fractionation for the different Fe/Sb ratios because the complexed forms and surface coverage did not vary. Previous studies also report the inner-sphere surface complex of Fh and Goe with Sb is unaffected by the Fe/Sb ratio.[6] However, Gou et al.[60] demonstrate using EXAFS that the difference in isotopic fractionation of Zn adsorbed on γ-Al_2O_3 is associated with surface coverage because the adsorption mechanism of Zn changed. In addition to controlling the metal species in the aqueous phase, pH can also affect surface coverage or mineral structure, resulting in a change in the adsorption mechanism. In this study, no significant differences in Sb isotope fractionation were observed in the adsorption edge experiments for each oxide, which indicates unchanged mineral—metal binding. Once the pH affects the adsorption mechanism of minerals on metals or changes the coordination environment between the aqueous and adsorbed phase, significant fractionation can occur and vary with pH. For example, the percentage of octahedral (bidentate binuclear complexes) involving Mo−Mn increases with decreasing pH when molybdenum is adsorbed on ferromanganese oxides, resulting in a significant decrease in molybdenum isotope fractionation.[61]

The adsorption of Sb by the three Fe (oxyhydr)oxides results in different Sb isotopic fractionation values, i.e., the Sb isotopic fractionation on Hem and Goe is more than double that on Fh, and further comparison of the adsorption mechanisms is necessary before analyzing the isotopic fractionation differences. In general, minerals with different structures affect isotopic fractionation due to the bond distance between the oxygen and metal atoms or variations of coordination, which relate to the metal bonding form. A significant difference in the Sb−Fe second-shell coordination environment in the Fe (oxyhydr)oxides was observed, with the second shell of Sb adsorbed on Hem and Goe involving fewer Fe atoms than Sb adsorbed on Fh. Limited Fe atoms are present in the second coordination shell of Hem and Goe, indicating the surface complexes are weaker and easier to enrich with light Sb isotopes, leading to larger isotopic fractionation than for Fh. Likewise, previous experiments show Ni adsorption on Goe results in greater isotope fractionation compared to Ni adsorption on Fh because the lower Ni−Fe coordination number of Goe allows the formation of weaker surface complexes, resulting in the enrichment of lighter Ni isotopes.[62] Interestingly, isotopic fractionation studies focusing on the adsorption of Zn,[63] Wu,[57] Ge,[58] and Cd[41] by different minerals (e.g., Fh, Goe, Hem, and MnO) add another perspective, i.e., that a key reason for the different fractionation by various minerals upon complexation is due to differences in the adsorbed and solid phases (e.g., octahedron vs. tetrahedron).

Environmental Implications. This study investigated the isotope fractionation during Sb adsorption on Fh, Hem, and Goe, with the results showing a close relation between Sb adsorption and its isotopic fractionation mechanisms at the solid/aqueous interface. In the natural environment, adsorption at the mineral/aqueous interface can significantly affect Sb isotope distribution. Fe (oxyhydr)oxides, which have a strong effect on Sb transport, are an important factor to consider with respect to Sb isotope fractionation. Similar to traditional metal stable isotopes, Sb isotopes can be applied in environmental geochemistry with respect to source and process tracing. Source tracing is appropriate for simple geochemical processes, and the contribution of different Sb sources can be obtained using a mixture model. Sb isotope source tracing has potential widespread applications once representative source isotopes are identified and if no overlapping effects with migrating isotopes are present. Further clarification is needed with respect to the magnitude of Sb isotopic fractionation in migration processes (e.g., the key process of Sb adsorption by Fe (oxyhydr)oxides). Process tracing refers to isotopic signature variations based on a specific or variable reaction; for example, soluble hexavalent chromium is reduced to precipitated trivalent chromium,[64] and the extent of the reaction can be quantified by isotope enrichment using a fractionation model. Further, Sb isotopic fractionation characterization using experimental methods is necessary before Sb isotopes can be applied for process tracing, which is one of the reasons we conducted this study. The results of this study on Sb isotopic fractionation behavior and mechanisms during adsorption by Fe (oxyhydr)oxides suggest Sb isotopes have the potential as effective tracers for studying the geochemical fate of Sb in the environment, whether via source or process tracing, which will aid in understanding Sb contamination in environmental systems. For example, our results will provide a reference for field studies of Sb isotopes in water or soil environments, including for the interpretation of previous studies on heavy Sb isotopes in drainage samples,[27,28] or for the understanding of Sb isotope changes in soils from the perspective of Sb adsorption by Fe (oxyhydr)oxides. However, samples of natural systems are complex, and the factors controlling Sb isotope fractionation are even more complex. Different control factors result in different isotopic fractionation magnitudes, and these fractionation effects often overlap, which brings challenges for future applications of Sb isotopes. Despite the contribution made by this study, systematic experimental studies of Sb isotope fractionation are still lacking. Future studies of Sb isotope fractionation are necessary to better define processes, including the effects of redox conditions on Sb, adsorption or co-precipitation of Sb with minerals, and the interaction of Sb with microorganisms and organic materials.

■ ASSOCIATED CONTENT

Supporting Information

The Supporting Information is available free of charge at https://pubs.acs.org/doi/10.1021/acs.est.3c01906.

> Synthesis and characterization of Fe (oxyhydr)oxides; adsorption kinetics, edge, and isotherm experimental data; fitting methods of adsorption kinetics and isotherm; Sb species calculation; detailed methods with the steps for column chemistry; EXAFS data collection, analysis, and evaluation; instrument parameters for Sb isotope measurements; and Sb isotopic composition and fitting methods (PDF)

■ AUTHOR INFORMATION

Corresponding Authors

Peng Liu − *School of Environmental Studies, China University of Geosciences, Wuhan 430074, China; Hubei Key Laboratory of Yangtze Catchment Environmental Aquatic Science, China University of Geosciences, Wuhan 430074, China; Key Laboratory of Mine Ecological Effects and System Restoration, Ministry of Natural Resources, Beijing 100081, China;* orcid.org/0000-0002-2870-7193; Email: pengliu@cug.edu.cn

Guangyi Sun − *State Key Laboratory of Environmental Geochemistry, Institute of Geochemistry, Chinese Academy of Sciences, Guiyang 550081, China;* orcid.org/0000-0001-8002-3576; Email: sunguangyi@mail.gyig.ac.cn

Authors

Weiqing Zhou − *School of Environmental Studies, China University of Geosciences, Wuhan 430074, China; Hubei Key Laboratory of Yangtze Catchment Environmental Aquatic Science, China University of Geosciences, Wuhan 430074, China; Key Laboratory of Mine Ecological Effects and System Restoration, Ministry of Natural Resources, Beijing 100081, China*

Jianwei Zhou − *School of Environmental Studies, China University of Geosciences, Wuhan 430074, China; Hubei Key Laboratory of Yangtze Catchment Environmental Aquatic Science, China University of Geosciences, Wuhan 430074, China; Key Laboratory of Mine Ecological Effects and System Restoration, Ministry of Natural Resources, Beijing 100081, China;* orcid.org/0000-0003-4952-4641

Xinbin Feng − *State Key Laboratory of Environmental Geochemistry, Institute of Geochemistry, Chinese Academy of Sciences, Guiyang 550081, China*

Bing Wen − *State Environmental Protection Key Laboratory of Soil Environmental Management and Pollution Control, Nanjing Institute of Environmental Sciences, Ministry of Ecology and Environment of China, Nanjing 210042, China*

Aiguo Zhou − *School of Environmental Studies, China University of Geosciences, Wuhan 430074, China*

Ziyi Zhou − *School of Environmental Studies, China University of Geosciences, Wuhan 430074, China*

Xin Liu − *Central-Southern Safety & Environment Technology Institute Co., Ltd., Wuhan 430000, China*

Complete contact information is available at: https://pubs.acs.org/10.1021/acs.est.3c01906

Notes

The authors declare no competing financial interest.

■ ACKNOWLEDGMENTS

This research was supported by the National Natural Science Foundation of China (42030706, 42277405, 42077182). X-ray absorption spectroscopy analyses were performed at Beamline 20-BM of the Advanced Photon Source, Argonne National Laboratory.

■ REFERENCES

(1) Fang, L.; Zhou, A.; Li, X.; Zhou, J.; Pan, G.; He, N. Response of antimony and arsenic in karst aquifers and groundwater geochemistry to the influence of mine activities at the world's largest antimony mine, central China. *J. Hydrol.* **2021**, *603*, No. 127131.

(2) Johnston, S. G.; Bennett, W. W.; Doriean, N.; Hockmann, K.; Karimian, N.; Burton, E. D. Antimony and arsenic speciation, redox-cycling and contrasting mobility in a mining-impacted river system. *Sci. Total Environ.* **2020**, *710*, No. 136354.

(3) Wen, B.; Zhou, J.; Zhou, A.; Liu, C.; Li, L. A review of antimony (Sb) isotopes analytical methods and application in environmental systems. *Int. Biodeterior. Biodegrad.* **2018**, *128*, 109−116.

(4) Peng, L.; Wang, N.; Xiao, T.; Wang, J.; Quan, H.; Fu, C.; Kong, Q.; Zhang, X. A critical review on adsorptive removal of antimony from waters: Adsorbent species, interface behavior and interaction mechanism. *Chemosphere* **2023**, 327, No. 138529.

(5) Ritchie, V. J.; Ilgen, A. G.; Mueller, S. H.; Trainor, T. P.; Goldfarb, R. J. Mobility and chemical fate of antimony and arsenic in historic mining environments of the Kantishna Hills district, Denali National Park and Preserve, Alaska. *Chem. Geol.* **2013**, *335*, 172−188.

(6) Mitsunobu, S.; Takahashi, Y.; Terada, Y.; Sakata, M. Antimony-(V) incorporation into synthetic ferrihydrite, goethite, and natural iron oxyhydroxides. *Environ. Sci. Technol.* **2010**, *44*, 3712−3718.

(7) Guo, X.; Wu, Z.; He, M.; Meng, X.; Jin, X.; Qiu, N.; Zhang, J. Adsorption of antimony onto iron oxyhydroxides: adsorption behavior and surface structure. *J. Hazard. Mater.* **2014**, *276*, 339−345.

(8) Scheinost, A. C.; Rossberg, A.; Vantelon, D.; Xifra, I.; Kretzschmar, R.; Leuz, A.-K.; Funke, H.; Johnson, C. A. Quantitative antimony speciation in shooting-range soils by EXAFS spectroscopy. *Geochim. Cosmochim. Acta* **2006**, *70*, 3299−3312.

(9) Essington, M. E.; Stewart, M. A. Adsorption of antimonate, sulfate, and phosphate by goethite: reversibility and competitive effects. *Soil Sci. Soc. Am. J.* **2018**, *82*, 803−814.

(10) Qiu, C.; Majs, F.; Douglas, T. A.; Schmidt, M.; Trainor, T. P. In situ structural study of Sb(V) adsorption on hematite (1102) using X-ray surface scattering. *Environ. Sci. Technol.* **2018**, *52*, 11161−11168.

(11) Mierzwa, J.; Mumbi, R.; Ray, A.; Rakshit, S.; Essington, M. E.; Sarkar, D. Antimony(V) adsorption at the hematite−water interface: a macroscopic and in situ ATR-FTIR study. *Soil Syst.* **2021**, *5*, 20.

(12) Rastegari, M.; Karimian, N.; Johnston, S. G.; Doherty, S. J.; Hamilton, J. L.; Choppala, G.; Hosseinpour Moghaddam, M.; Burton, E. D. Antimony(V) incorporation into schwertmannite: critical insights on antimony retention in acidic environments. *Environ. Sci. Technol.* **2022**, *56*, 17776−17784.

(13) Karimian, N.; Johnston, S. G.; Tavakkoli, E.; Frierdich, A. J.; Burton, E. D. Mechanisms of arsenic and antimony co-sorption onto jarosite: an x-ray absorption spectroscopic study. *Environ. Sci. Technol.* **2023**, *57*, 4813−4820.

(14) Berglund, M.; Wieser, M. E. Isotopic compositions of the elements 2009 (IUPAC Technical Report). *Pure Appl. Chem.* **2010**, *83*, 397−410.

(15) Rouxel, O.; Ludden, J.; Fouquet, Y. Antimony isotope variations in natural systems and implications for their use as geochemical tracers. *Chem. Geol.* **2003**, *200*, 25−40.

(16) Asaoka, S.; Takahashi, Y.; Araki, Y.; Tanimizu, M. Preconcentration method of antimony using modified thiol cotton fiber for isotopic analyses of antimony in natural samples. *Anal. Sci.* **2011**, *27*, 25−28.

(17) Liu, J.; Chen, J.; Zhang, T.; Wang, Y.; Yuan, W.; Lang, Y.; Tu, C.; Liu, L.; Birck, J.-L. Chromatographic purification of antimony for accurate isotope analysis by MC-ICP-MS. *J. Anal. At. Spectrom.* **2020**, *35*, 1360−1367.

(18) Colin, F.; Eléonore, R.; Rémi, F.; Corinne, C. A single-step purification method for the precise determination of the antimony isotopic composition of environmental, geological and biological samples by HG-MC-ICP-MS. *J. Anal. At. Spectrom.* **2021**, *36*, 776−785.

(19) Li, S.; Deng, Y.; Zheng, H.; Liu, X.; Tang, P.; Zhou, J.; Zhu, Z. A new purification method based on a thiol silica column for high precision antimony isotope measurements. *J. Anal. At. Spectrom.* **2021**, *36*, 157−164.

(20) Sun, G.; Wu, Y.; Feng, X.; Wu, X.; Li, X.; Deng, Q.; Wang, F.; Fu, X. Precise analysis of antimony isotopic composition in geochemical materials by MC-ICP-MS. *Chem. Geol.* **2021**, *582*, No. 120459.

(21) Zhang, C.; Sun, G.; Li, X.; Wu, Y.; Yao, H.; Huang, J.-H.; Feng, X. Sampling and determination of antimony isotopes in airborne particles: an assessment of membrane filter materials. *J. Anal. At. Spectrom.* **2022**, *37*, 2713−2720.

(22) Lobo, L.; Devulder, V.; Degryse, P.; Vanhaecke, F. Investigation of natural isotopic variation of Sb in stibnite ores via multi-collector ICP-mass spectrometry − perspectives for Sb isotopic analysis of Roman glass. *J. Anal. At. Spectrom.* **2012**, *27*, 1304.

(23) Lobo, L.; Degryse, P.; Shortland, A.; Vanhaecke, F. Isotopic analysis of antimony using multi-collector ICP-mass spectrometry for provenance determination of Roman glass. *J. Anal. At. Spectrom.* **2013**, *28*, 1213−1219.

(24) Lobo, L.; Degryse, P.; Shortland, A.; Eremin, K.; Vanhaecke, F. Copper and antimony isotopic analysis via multi-collector ICP-mass spectrometry for provenancing ancient glass. *J. Anal. At. Spectrom.* **2014**, *29*, 58−64.

(25) Degryse, P.; Lobo, L.; Shortland, A.; Vanhaecke, F.; Blomme, A.; Painter, J.; Gimeno, D.; Eremin, K.; Greene, J.; Kirk, S.; Walton, M. Isotopic investigation into the raw materials of Late Bronze Age glass making. *J. Archaeol. Sci.* **2015**, *62*, 153−160.

(26) Resongles, E.; Freydier, R.; Casiot, C.; Viers, J.; Chmeleff, J.; Elbaz-Poulichet, F. Antimony isotopic composition in river waters affected by ancient mining activity. *Talanta* **2015**, *144*, 851−861.

(27) Tanimizu, M.; Araki, Y.; Asaka, S.; Takahashi, Y. Determination of natural isotopic variation in antimony using inductively coupled plasma mass spectrometry for an uncertainty estimation of the standard atomic weight of antimony. *Geochem. J.* **2011**, *45*, 27−32.

(28) Wen, B.; Zhou, J.; Tang, P.; Jia, X.; Zhou, W.; Huang, J. Antimony (Sb) isotopic signature in water systems from the world's largest Sb mine, central China: novel insights to trace Sb source and mobilization. *J. Hazard. Mater.* **2023**, *446*, No. 130622.

(29) Ferrari, C.; Méheut, M.; Resongles, E.; Freydier, R.; Casiot, C. Equilibrium mass-dependent isotope fractionation of antimony between stibnite and Sb secondary minerals: a first-principles study. *Chem. Geol.* **2022**, *611*, No. 121115.

(30) Zhai, D.; Mathur, R.; Liu, S.-A.; Liu, J.; Godfrey, L.; Wang, K.; Xu, J.; Vervoort, J. Antimony isotope fractionation in hydrothermal systems. *Geochim. Cosmochim. Acta* **2021**, *306*, 84−97.

(31) Zhou, W.; Zhou, A.; Wen, B.; Liu, P.; Zhu, Z.; Finfrock, Z.; Zhou, J. Antimony isotope fractionation during adsorption on aluminum oxides. *J. Hazard. Mater.* **2022**, *429*, No. 128317.

(32) Cornell, R. M.; Schwertmann, U. *The Iron Oxides Structure: Properties, Reaction, Occurences and Uses*; Wiley-VCH: Weinheim, 2003.

(33) Watkins, R.; Weiss, D.; Dubbin, W.; Peel, K.; Coles, B.; Arnold, T. Investigations into the kinetics and thermodynamics of Sb(III) adsorption on goethite (α-FeOOH). *J. Colloid Interface Sci.* **2006**, *303*, 639−646.

(34) Ravel, B.; Newville, M. ATHENA, ARTEMIS, HEPHAESTUS: data analysis for X-ray absorption spectroscopy using IFEFFIT. *J. Synchrotron Radiat.* **2005**, *12*, 537−541.

(35) Downs, R. T.; Hall-Wallace, M. The American mineralogist crystal structure database. *Am. Mineral.* **2003**, *88*, 247−250.

(36) Ye, Z.; Zhou, J.; Liao, P.; Finfrock, Y. Z.; Liu, Y.; Shu, C.; Liu, P. Metal (Fe, Cu, and As) transformation and association within secondary minerals in neutralized acid mine drainage characterized using X-ray absorption spectroscopy. *Appl. Geochem.* **2022**, *139*, No. 105242.

(37) Zhou, Z.; Liu, P.; Wang, S.; Finfrock, Y. Z.; Ye, Z.; Feng, Y.; Li, X. Iron-modified biochar-based bilayer permeable reactive barrier for Cr(VI) removal. *J. Hazard. Mater.* **2022**, *439*, No. 129636.

(38) He, Z.; Liu, R.; Liu, H.; Qu, J. Adsorption of Sb(III) and Sb(V) on freshly prepared ferric hydroxide (FeOxHy). *Environ. Eng. Sci.* **2015**, *32*, 95−102.

(39) Hudcová, B.; Erben, M.; Vitkova, M.; Komarek, M. Antimonate adsorption onto Mg-Fe layered double hydroxides in aqueous solutions at different pH values: Coupling surface complexation modeling with solid-state analyses. *Chemosphere* **2019**, *229*, 236−246.

(40) Gheju, M.; Balcu, I.; Mosoarca, G. Removal of Cr(VI) from aqueous solutions by adsorption on MnO_2. *J. Hazard. Mater.* **2016**, *310*, 270−277.

(41) Yan, X.; Zhu, M.; Li, W.; Peacock, C. L.; Ma, J.; Wen, H.; Liu, F.; Zhou, Z.; Zhu, C.; Yin, H. Cadmium isotope fractionation during adsorption and substitution with iron (oxyhydr)oxides. *Environ. Sci. Technol.* **2021**, *55*, 11601−11611.

(42) Liu, X.; Zhou, J.; Zhou, W.; Feng, Y.; Finfrock, Y. Z.; Liu, Y.; Liu, P.; Shu, C. Efficiency and mechanisms of Sb(III/V) removal by Fe-modified biochars using X-ray absorption spectroscopy. *J. Environ. Chem. Eng.* **2021**, *9*, No. 106741.

(43) Rehr, J. J.; Albers, R. C. Theoretical approaches to X-ray absorption fine structure. *Rev. Mod. Phys.* **2000**, *72*, 621−654.

(44) Leuz, A. K.; Monch, H.; Johnson, C. A. Sorption of Sb(III) and Sb(V) to goethite: Influence on Sb(III) oxidation and mobilization. *Environ. Sci. Technol.* **2006**, *40*, 7277−7282.

(45) Wasylenki, L. E.; Swihart, J. W.; Romaniello, S. J. Cadmium isotope fractionation during adsorption to Mn oxyhydroxide at low and high ionic strength. *Geochim. Cosmochim. Acta* **2014**, *140*, 212−226.

(46) Wiederhold, J. G. Metal stable isotope signatures as tracers in environmental geochemistry. *Environ. Sci. Technol.* **2015**, *49*, 2606−2624.

(47) Liu, J.; Sheng, A.; Li, X.; Arai, Y.; Ding, Y.; Nie, M.; Yan, M.; Rosso, K. M. Understanding the importance of labile Fe(III) during Fe(II)-catalyzed transformation of metastable iron oxyhydroxides. *Environ. Sci. Technol.* **2022**, *56*, 3801−3811.

(48) Schauble, E. A. Applying stable isotope fractionation theory to new systems. *Rev. Mineral. Geochem.* **2004**, *55*, 65−111.

(49) Balistrieri, L. S.; Borrok, D. M.; Wanty, R. B.; Ridley, W. I. Fractionation of Cu and Zn isotopes during adsorption onto amorphous Fe(III) oxyhydroxide: Experimental mixing of acid rock drainage and ambient river water. *Geochim. Cosmochim. Acta* **2008**, *72*, 311−328.

(50) Li, X. F.; Liu, Y. First-principles study of Ge isotope fractionation during adsorption onto Fe(III)-oxyhydroxide surfaces. *Chem. Geol.* **2010**, *278*, 15−22.

(51) Xu, W. P.; Zhu, J. M.; Johnson, T. M.; Wang, X. L.; Lin, Z. Q.; Tan, D. C.; Qin, H. B. Selenium isotope fractionation during adsorption by Fe, Mn and Al oxides. *Geochim. Cosmochim. Acta* **2020**, *272*, 121−136.

(52) Wasylenki, L. E.; Weeks, C. L.; Bargar, J. R.; Spiro, T. G.; Hein, J. R.; Anbar, A. D. The molecular mechanism of Mo isotope fractionation during adsorption to birnessite. *Geochim. Cosmochim. Acta* **2011**, *75*, 5019−5031.

(53) Tanaka, M.; Ariga, D.; Kashiwabara, T.; Takahashi, Y. Adsorption mechanism of molybdenum(VI) on manganese oxides causing a large isotope fractionation. *ACS Earth Space Chem.* **2018**, *2*, 1187−1195.

(54) Brennecka, G. A.; Wasylenki, L. E.; Bargar, J. R.; Weyer, S.; Anbar, A. D. Uranium isotope fractionation during adsorption to Mn-oxyhydroxides. *Environ. Sci. Technol.* **2011**, *45*, 1370−1375.

(55) Wasylenki, L. E.; Rolfe, B. A.; Weeks, C. L.; Spiro, T. G.; Anbar, A. D. Experimental investigation of the effects of temperature and ionic strength on Mo isotope fractionation during adsorption to manganese oxides. *Geochim. Cosmochim. Acta* **2008**, *72*, 5997−6005.

(56) Goldberg, T.; Archer, C.; Vance, D.; Poulton, S. W. Mo isotope fractionation during adsorption to Fe (oxyhydr)oxides. *Geochim. Cosmochim. Acta* **2009**, *73*, 6502−6516.

(57) Kashiwabara, T.; Kubo, S.; Tanaka, M.; Senda, R.; Iizuka, T.; Tanimizu, M.; Takahashi, Y. Stable isotope fractionation of tungsten during adsorption on Fe and Mn (oxyhydr)oxides. *Geochim. Cosmochim. Acta* **2017**, *204*, 52−67.

(58) Pokrovsky, O. S.; Galy, A.; Schott, J.; Pokrovski, G. S.; Mantoura, S. Germanium isotope fractionation during Ge adsorption on goethite and its coprecipitation with Fe oxy(hydr)oxides. *Geochim. Cosmochim. Acta* **2014**, *131*, 138−149.

(59) Wasylenki, L. E.; Schaefer, A. T.; Chanda, P.; Farmer, J. C. Differential behavior of tungsten stable isotopes during sorption to Fe versus Mn oxyhydroxides at low ionic strength. *Chem. Geol.* **2020**, *558*, No. 119836.

(60) Gou, W.; Li, W.; Ji, J.; Li, W. Zinc isotope fractionation during sorption onto Al oxides: atomic level understanding from EXAFS. *Environ. Sci. Technol.* **2018**, *52*, 9087−9096.

(61) Kashiwabara, T.; Takahashi, Y.; Tanimizu, M.; Usui, A. Molecular-scale mechanisms of distribution and isotopic fractionation of molybdenum between seawater and ferromanganese oxides. *Geochim. Cosmochim. Acta* **2011**, *75*, 5762−5784.

(62) Gueguen, B.; Sorensen, J. V.; Lalonde, S. V.; Peña, J.; Toner, B. M.; Rouxel, O. Variable Ni isotope fractionation between Fe-oxyhydroxides and implications for the use of Ni isotopes as geochemical tracers. *Chem. Geol.* **2018**, *481*, 38−52.

(63) Juillot, F.; Maréchal, C.; Ponthieu, M.; Cacaly, S.; Morin, G.; Benedetti, M.; Hazemann, J. L.; Proux, O.; Guyot, F. Zn isotopic fractionation caused by sorption on goethite and 2-Lines ferrihydrite. *Geochim. Cosmochim. Acta* **2008**, *72*, 4886−4900.

(64) Shrimpton, H. K.; Jamieson-Hanes, J. H.; Ptacek, C. J.; Blowes, D. W. Real-time XANES measurement of Se reduction by zerovalent iron in a flow-through cell, and accompanying Se isotope measurements. *Environ. Sci. Technol.* **2018**, *52*, 9304−9310.